Ion-electron recombination in merged-beams experiments

Henning T. Schmidt

Institute of Physics and Astronomy,
Aarhus University.
1994

Table of Contents

1. ***Preface*** *2*

2. ***Introduction*** *6*

3. ***The Merged-Beams Experiments*** *9*

3.1.	*The ion beams*	*10*
3.2.	*The electron beams*	*14*
3.3.	*Electron cooling*	*29*

4. ***Radiative Recombination*** *35*

4.1	*RR for fully stripped ions*	*35*
4.2	*RR for non-fully stripped ions*	*39*
4.3	*Laser induced RR*	*42*

5. ***Dielectronic Recombination*** *47*

5.1	*Introduction to DR*	*47*
5.2	*DR for ground state Li-like ions*	*52*
5.3	*DR for metastable He-like ions (the single-pass experiment)*	*57*
5.4	*DR for metastable He-like ions (the TSR experiment)*	*67*
5.5	*DR for Be-, B-, and C-like ions*	*74*

6. ***Lifetime measurements based on DR*** *77*

6.1	*Lifetime of the ^3S metastable state of He-like ions*	*77*
6.2	*The experiment*	*79*
6.3	*Analysis of data from the decay rate measurement*	*82*
6.4	*Discussion of the results*	*88*

7. ***Dissociative Recombination*** *94*

7.1	*Earlier DisR experiments*	*94*
7.2	*Some basic concepts of diatomic molecules*	*96*
7.3	*The DisR processes*	*101*
7.4	*The ASTRID H_2^+ experiment*	*106*
7.5	*Results and discussion*	*112*

8. ***Summary*** *121*

9. ***Dansk resumé*** *123*

10. ***Acknowledgments*** *125*

1. Preface

The present thesis serves to fulfil the requirements for the Ph.D. degree at the Faculty of Natural Sciences, Aarhus University. The thesis presents merged-beams experiments, investigating processes of ion-electron recombination. The main part of the work described was performed with the electron cooler at the Institute of Physics and Astronomy, Aarhus University, but the results of a six-month stay at the Max-Planck-Institut (MPI) für Kernphysik in Heidelberg, Germany, are presented as well.

When in the mid-80s, it was decided to build the Aarhus STorage RIng, Denmark (ASTRID), a wise and fruitful decision of building first the electron cooler and installing it at the TANDEM accelerator was made. This way one could gain experience working with ultra-high vacuum systems before constructing the storage ring itself, and at the same time provide an excellent tool for the study of recombination between free electrons and multiply charged ions in a single-pass configuration. Indeed, impressive results were obtained. The first direct tests of the absolute cross sections for radiative recombination (RR) were performed (Andersen 1990), and the dielectronic recombination (DR) measurements (Andersen 1989) had an energy resolution improved by a factor of 30 compared to earlier works.

When I joined the project as a student in the Fall of 1989, these two great successes had been achieved quite recently, and in the spirit of optimism that followed, we decided to try to perform laser-induced radiative recombination (LIR). This attempt was not successful, and after observations of LIR were reported from MPI, Heidelberg

(Schramm 1991) and from University of Western Ontario (Yousif 1991), we stopped this experiment. During the time of our LIR experiment, we continued to study RR for non-fully stripped ions [II,V] and DR with low-energy electrons [I,III,IV,V]. In the Spring of 1992, the electron cooler was 'recombined' with ASTRID. In the following year, technical difficulties had to be solved, and no real electron-cooler experiments were performed. During this year, I spent six months in Heidelberg working on DR with metastable He-like ions measured both as a function of electron energy and as a function of time after injection to deduce the lifetimes of the metastable 1s2s ^{3}S states [VI]. In 1993 we made the first experiments with the electron cooler at ASTRID. So far, we have studied electron cooling of D^+, dissociative recombination (DisR) of H_2^+, and electron-impact detachment of D^-. For future applications of the electron cooler, we have improved the energy resolution at low relative energies by about one order of magnitude, applying the so-called 'adiabatic expansion' technique first realized at the Stockholm storage ring CRYRING (Danared 1993).

Throughout this thesis, a rather significant variation concerning the amount of details presented on the performance and results of the different experiments will encounter the reader. This is due to a selection based on the following criteria: First of all, previously unpublished material, in particular sec.5.4 on the TSR measurement of DR for metastable He-like ions and ch.7 on the ASTRID experiment on DisR of H_2^+, is given a high priority. Other criteria also considered in the selection process are the existence of detailed theoretical predictions to compare with our data and the usefulness of a certain

detail in making a point in the presentation.

Parts of the material considered in this thesis has previously been presented in the publications listed in the following.

I. N R Badnell, M S Pindzola, L H Andersen, J Bolko, and H T Schmidt (1991): *Dielectronic recombination of light Be-like and B-like ions.* Journal of Physics B **24** 4441

II. L H Andersen, G Y Pan, and H T Schmidt (1992): *Radiative recombination with highly charged Si^{6+} and Si^{11+} ions.* Journal of Physics B **25** 277

III. L H Andersen, G Y Pan, H T Schmidt, N R Badnell, and M S Pindzola (1992): *State-selective measurements and calculations of dielectronic recombination with Li-like N^{4+},F^{6+} and Si^{11+} ions.* Physical Review A **45** 6332

IV. L H Andersen, G Y Pan, H T Schmidt, N R Badnell, and M S Pindzola (1992): *Absolute measurements and calculations of dielectronic recombination with metastable He-like N,F and Si ions.* Physical Review A **45** 7868

V. H T Schmidt, G Y Pan, and L H Andersen (1992): *Dielectronic recombination with $\Delta n=0$ and $\Delta n=1$ core excitations and radiative recombination for C-like F^{3+} ions.* Journal of Physics B **25** 3165

VI. H T Schmidt, P Forck, M Grieser, D Habs, J Kenntner, G Miersch, R Repnow, U Schramm, T Schüβler, D Schwalm, and A Wolf (1994): *High-precision measurement of the relativistic magnetic-dipole decay rate of metastable heliumlike carbon ions in a storage ring.* Phys.Rev.Lett. **72**, 1616

The papers listed above will be referred to by roman numbers, whereas other literature cited in the text is referred to by the name of the first author followed by the year of publication. References to other literature will be given at the end of each chapter.

L H Andersen, J Bolko, P Kvistgaard (1990) Phys.Rev.Lett. ***64*** *729.*

L H Andersen, P Hvelplund, H Knudsen, and P Kvistgaard (1989) Phys.Rev.Lett. ***62*** *2656*

U Schramm, J Berger, M Grieser, D Habs, E Jaeschke, G Kilgus, D Schwalm, A Wolf, R Neumann, R Schuch (1991) Phys.Rev.Lett. ***67*** *22*

F B Yousif, P v.d. Donk, Z Kucherowski, J Reis, E Brannen, J B A Mitchell, and T J Morgan (1991) Phys.Rev.Lett. ***67*** *26*

H Danared (1993) NIM A335 397

2. Introduction

From our every-day experience, we all know that matter is found in three phases: The solid phase, the liquid phase, and the gaseous phase. In the ordinary gas phase, matter consists of free neutral molecules. In the situation, where some degree of ionization has taken place, and we have a mixture of atomic and molecular ions and free electrons, we speak of a fourth phase, the plasma phase.

The plasma phase can be reached either by having a very high temperature or by introducing some external ionization mechanism, such as an electrical discharge or irradiation with light with a photon energy exceeding a few eV (i.e. UV, x rays, and γ rays).

When a plasma has been formed, an equilibrium situation can be reached:

$$X^{q+} + e^- \rightleftharpoons X^{(q-1)+} + \text{energy (e.g. photons)},$$

where X^{q+} denotes an ion in charge state q+. The process from right to left is ionization, while the inverse process is ion-electron recombination, the subject of this thesis. Of course, in a plasma many other processes take place (ion-ion charge exchange, ion excitation induced by collisions with electrons, emission of bremsstrahlung from electrons accelerated by ions, etc.). However, ion-electron recombination remains an essential feature of plasma physics. Plasmas, where these 'atomic physics' processes are dominating, are well known in nature. They can be found in, e.g., stellar atmospheres and in interstellar nebulae; but also in the upper atmosphere of the Earth, where the solar UV radiation leads to ionization. In fact, some of the first experimental

investigations of ion-electron recombination were performed as an attempt to understand the number densities of atomic and molecular ions in the upper atmosphere.

Let us now consider a system consisting of an ion X^{q+} and a free electron e^-. By the conventional definition of the zero point for the total mechanical energy, this system must have a positive energy, while a system forming a stable, bound state of the two (i.e. $X^{(q-1)+}$) must have a negative energy. Hence, in a recombination process, energy in some form must be released. In radiative recombination (RR), the excess energy is emitted in the form of a photon. This is a non-resonant process, having its maximum rate at 0 eV relative energy. Since this process does not require any change of the structure of the initial ion, this will be possible for any positive ion, even a fully stripped one. Another process, also possible for any ion, is referred to as three-body (or ternary) recombination (TR). In this process, the excess energy is given to a second free electron in the form of kinetic energy. Since this process requires the presence of two free electrons, it will have a rate proportional to the electron density n_e squared. This means that when the electron density becomes sufficiently high, the TR rate (which also takes on its maximum value at zero relative energy) will exceed the RR rate. However, for the experiments described in this thesis, the electron density is sufficiently low that the TR contribution is negligible.

For ions carrying electrons, a third recombination mechanism, known as dielectronic recombination (DR), becomes possible. Here the excess energy in the recombination process is used to excite one of the bound electrons, leaving the ion in a doubly excited state which might

autoionize or, alternatively, stabilize radiatively, in which case the DR process has been completed. Since the excitation of the initially bound electron requires a specific amount of energy, the DR process will be resonant.

When the ion, in the initial state, is a molecular ion, new degrees of freedom describing the relative motion of the nuclei are introduced. This makes possible a fourth recombination mechanism, for which the excess energy is transferred to these new degrees of freedom. As a consequence of this, the molecule dissociates. This process is therefore called dissociative recombination.

3. The Merged-Beams Experiments

In this chapter, general features of the merged-beams experiments will be described, postponing some experimental points to the chapters concerning the particular experiments. In sec.3.1 the accelerators and ion beams are briefly described, emphasizing the features relevant to the electron-cooler experiments. Section 3.2 deals with the electron cooler. The electron beam will be described in much more detail than the ion beam since it is the velocity spread of the electrons that determines the energy resolution in the experiments. The final section of this chapter is devoted to electron cooling which, besides being an interesting physical process in itself, is an important tool for understanding other merged-beams experiments performed in storage rings.

The general idea of merged-beams recombination measurements is to overlap two co-propagating beams of electrons and ions of charge q times the elementary charge e over a certain interaction region, and then, as a function of the relative energy, monitor the yield of ions in charge state (q−1)+. The entity determined in the experiments is the recombination rate coefficient $\langle v\sigma \rangle$ (see sec.3.2 eq.3.5). The experimental rate coefficient is determined as

$$\langle v\sigma \rangle = \frac{N^{(q-1)+} - N_0^{(q-1)+}}{N^{q+}} \frac{v_i}{Ln_e\varepsilon}, \qquad \textbf{(3.1)}$$

where $N^{(q-1)+}$ is the yield of ions in the (q−1)+ charge state, with the electron beam tuned to the desired relative energy, $N_0^{(q-1)+}$ is a background measurement performed by switching off the ion beam (chopping), or changing the energy to a value with zero rate coefficient

(modulating) or, in the case of the storage ring, DR measurements for ions in metastable states waiting for the metastable component to decay to the ground state. L is the length of the interaction region, n_e is the electron density, ε is the detector efficiency, and v_i is the ion velocity in the laboratory rest frame.

3.1. The ion beams

The single-pass experiments [I-V] were performed at the Aarhus 6 MV Tandem accelerator. The setup is sketched in fig. 3.1. Positively charged atomic ions were available with typical currents in the range of 200 nA to about 1 μA for energies of 1-2 MeV per atomic mass unit. From the bending magnet before the electron cooler and on, the pressure was kept below $1\text{-}2\cdot10^{-11}$ mBar to reduce the background signal caused by electron capture in collisions with residual-gas molecules. In the interaction region, two sets of electro-static pick-up

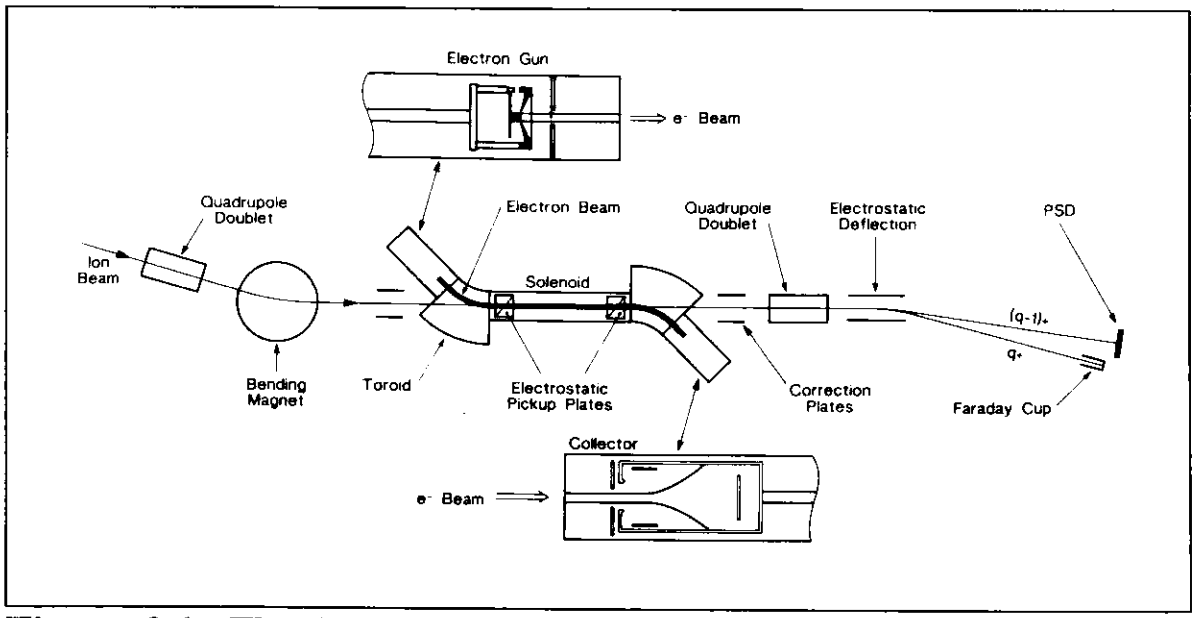

Figure 3.1 *The Aarhus single-pass experiment.*

plates were used to monitor the positions of both the ion and electron beams to ensure full overlap. The ion beam was assumed to be gaussian with a FWHM of 2-3 mm, and the electron beam was 1 cm diameter with uniform density. After the electron cooler, a charge-state separation was performed using a transverse electric field, typically of the order of 10 kV/cm. As a consequence of the traversal of this field, electrons in high Rydberg states were field-ionized and therefore not counted as recombined. The critical principal quantum number, n_{limit}, above which ionization takes place, is given by the following semi-classical expression (Griffin 1989)

$$n_{\text{limit}} = (6.2 \cdot 10^8 \ q^3/E)^{1/4}, \qquad \textbf{(3.2)}$$

where E is the electric-field strength in V/cm. To facilitate the detection, it was necessary to focus the final-state ions onto the position-sensitive channel-plate detector, and therefore no experiments with singly charged ions could be performed since these would result in neutral products.

Figure 3.2 shows the storage ring ASTRID with the parts of greatest interest to the electron-cooler experiments. Beams of singly charged, positive and negative, atomic and molecular ions covering a mass range of 1-1000 atomic mass units have been stored at the injection energy of 50 to 200 keV. However, to perform electron cooler experiments, it is necessary to increase the energy to several MeV, depending on the specific ion beam. The acceleration is achieved by bunching the beam with the RF cavity and then perform a synchronized ramping of the magnetic-dipole fields of the storage ring and the RF frequency. During this ramping, it is necessary to monitor the

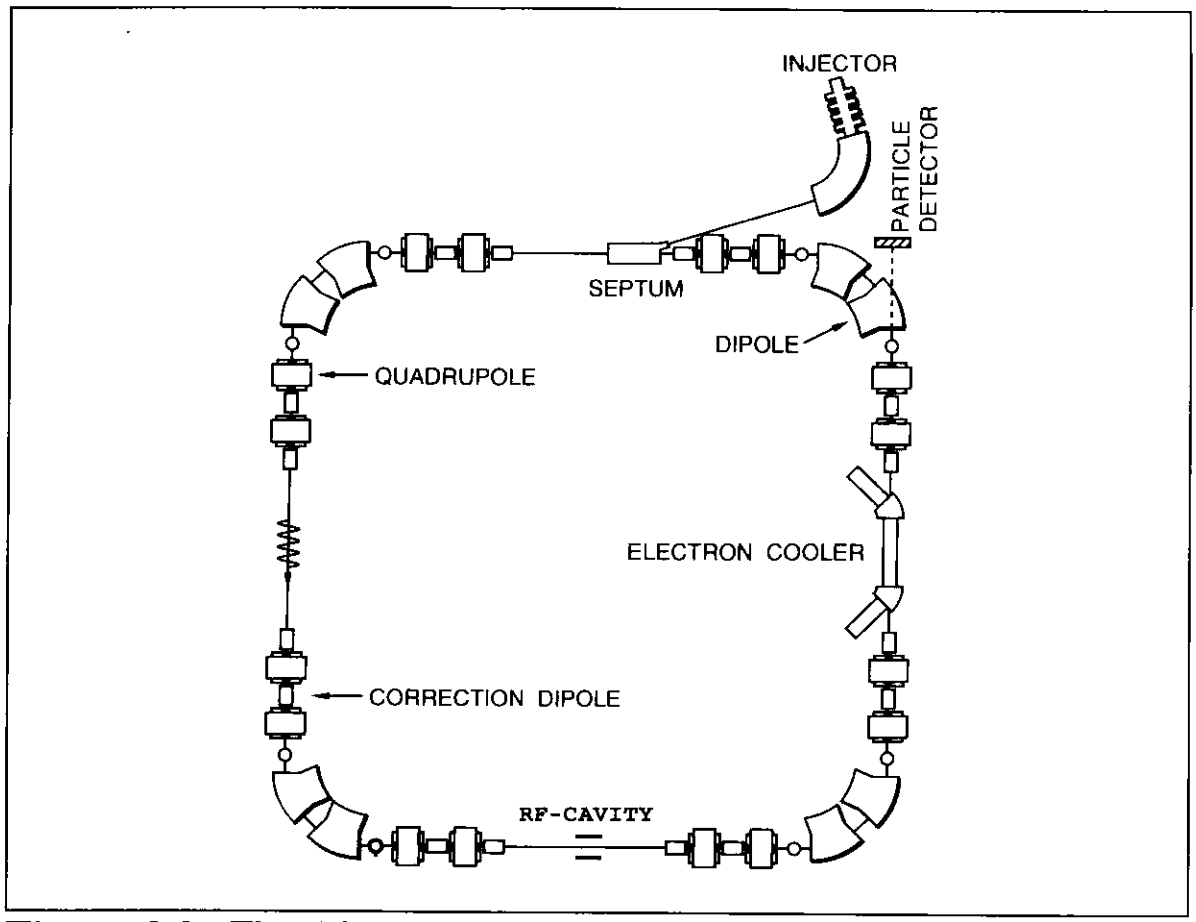

Figure 3.2 *The ASTRID storage ring.*

time structure of the ion beam on one of the pick-up plates to keep the relative phase of the RF and the ion bunches fixed. To perform this monitoring, an ion current of 0.5-1 μA is required. Due to losses during storage and acceleration, it is therefore only possible to perform electron-cooler experiments with ions for which currents from the ion sources of a few μA's are achievable. For many singly charged positive ions, currents of this magnitude are available from the 'universal' standard plasma ion sources ('Nielsen'-sources). For some negative ions, sputter ion sources (e.g. O^-) or duoplasmatrons (e.g. H^-) can yield the necessary current. An EBIS (Electron Beam Ion Source) that can yield high currents of multiply charged ions is under construction and will be available for future experiments. The ion-beam

position is monitored by the ten sets of electrostatic pick-up plates; two in the electron cooler and one at each end of the four straight sections. The positions can be optimized by adjusting the eight correction dipoles. Charge-state analysis is inherently performed in the dipole magnet following the electron cooler. The effective electric field caused by the transverse magnetic field will lead to field ionization of ions in high Rydberg states according to eq.(3.2). In SI units, the field strength is given as

$$E = \gamma vB = \frac{vB}{\sqrt{1-v^2/c^2}}, \qquad \textbf{(3.3)}$$

where v is the ion velocity. This electric field is typically of the order of 100 kV/cm.

As mentioned in the preface, some of the experiments described in this thesis were performed at the TSR (Test Storage Ring) at the Max-Planck-Institut für Kernphysik in Heidelberg. At the TSR, ions can be injected from a 12 MV Tandem accelerator. This means that electron-cooler experiments can be performed at the injection energy. This point was crucial to these experiments since they concerned ions in metastable states with lifetimes in the millisecond range, leaving no time for ion-beam acceleration. Like in ASTRID, the dipole magnet following the electron cooler acts as a charge-state analyzer. This means that field ionization according to eqs. (3.2) and (3.3) takes place.

3.2 The electron beams

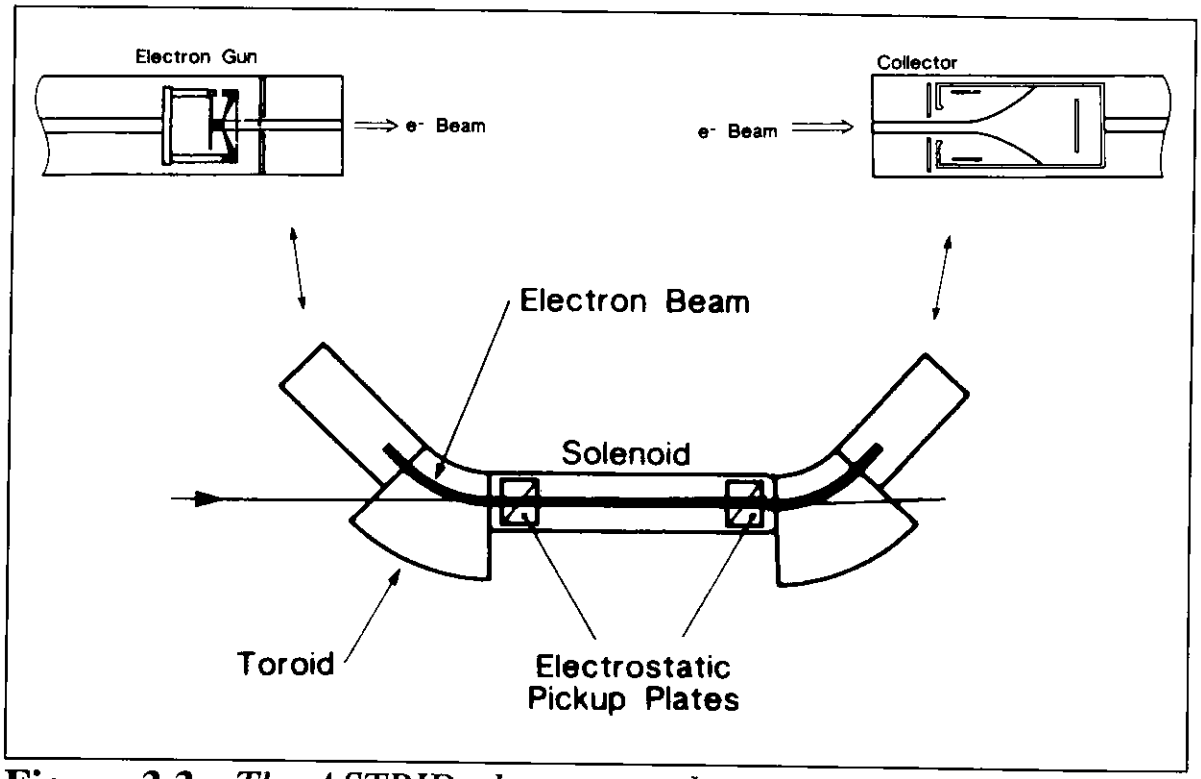

Figure 3.3 *The ASTRID electron cooler.*

Figure 3.3 shows schematically the ASTRID electron cooler. The source of electrons is an indirectly heated disc-shaped BaO-coated tungsten cathode. Cathodes of 10 and 15 mm diameter have been used. The cathode is surrounded by a Pierce shield which can be given a low bias voltage with respect to the cathode potential. From the cathode, the electrons are accelerated towards the anode which is a grid with approximately 80% transmittance. In the case of a space-charge-limited electron beam, the emitted electron current is given by (Poth 1990)

$$I_{electron} = PV^{3/2}, \qquad (3.4)$$

where V is the cathode-anode potential difference, and the constant of proportionality P (the perveance) is inversely proportional to the square

of the cathode-anode distance which can be varied from the outside, allowing for continuous electron-current tuning. The electron beam is guided from the electron gun through the one-meter interaction region to the collector by a solenoid magnetic field. In standard operation, this field is kept constant from the electron gun to the entrance of the collector, leading to a constant beam diameter equal to the cathode diameter. In the collector, the solenoid field decreases, and the beam blows up transversely.

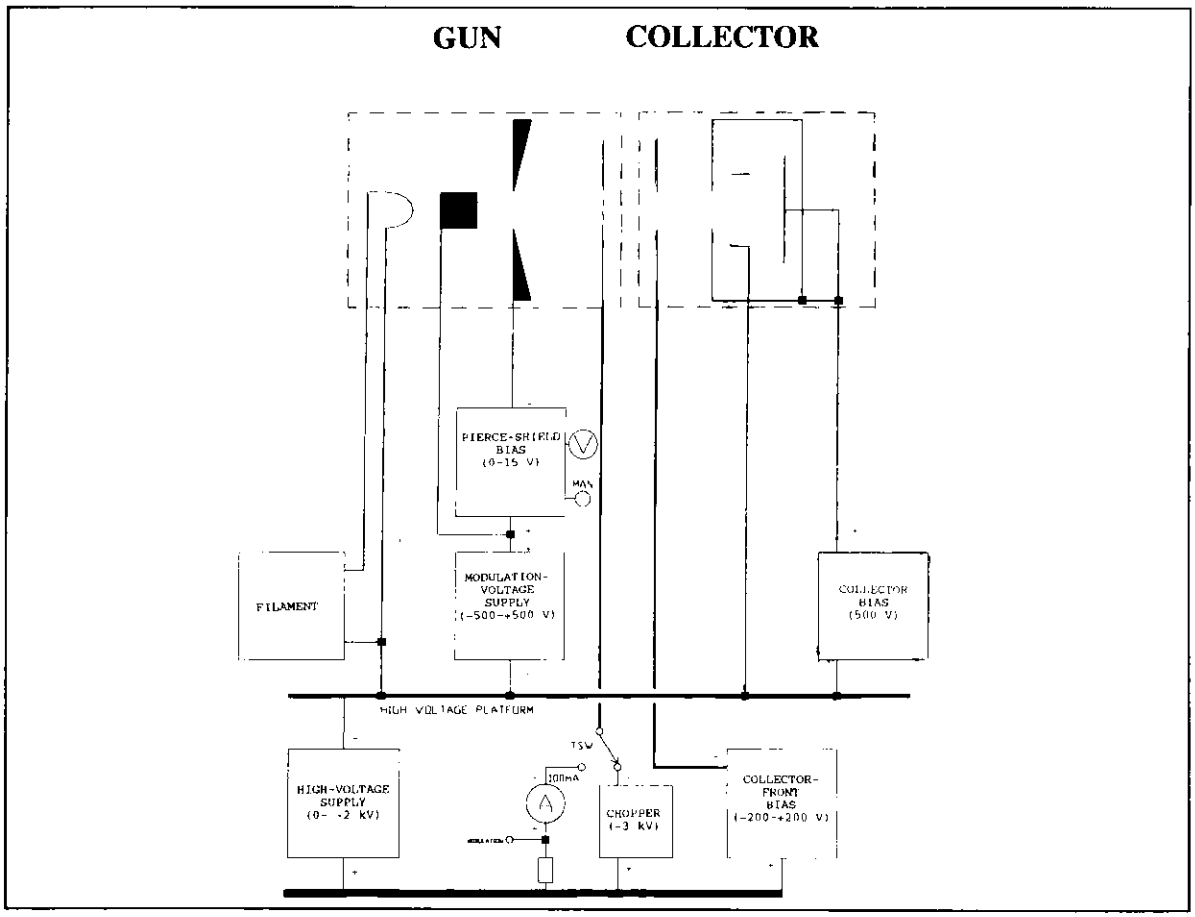

Figure 3.4 *The electrical connections for the electron cooler.*

In fig.3.4 is shown the electrical connections for the electron cooler. The cooler can be run in a DC mode, where the high-voltage platform voltage is equal to the acceleration voltage, but it is often useful to be able to modulate the acceleration voltage between two

values or to switch the beam on and off. For modulation, we have a ±500 V supply at the high-voltage platform, and for chopping the beam we have a 3 kV supply connected to the anode.

In the remainder of this section, I will discuss the electron-beam velocity distribution since the influence of the ion-velocity distribution on the distribution of relative velocities can be neglected due to the much larger mass of the ions. If the total cross section for recombination as a function of the relative velocity v is known, the rate coefficient $\langle v\sigma \rangle$ in a merged-beams experiment may be expressed as

$$\langle v\sigma \rangle = \int v\, \sigma(v)\, f\left(\bar{v},\Delta,T_{\perp},T_{\parallel}\right) d\bar{v}. \qquad \textbf{(3.5)}$$

Here the electron-velocity distribution f in the ion-beam rest frame is a flattened Maxwell distribution, i.e., the product of a two-dimensional transverse and a one-dimensional longitudinal, gaussian velocity distribution,

$$f\left(\bar{v},\Delta,T_{\perp},T_{\parallel}\right) = \frac{m}{2\pi k T_{\perp}} \exp\frac{-mv_{\perp}^2}{2kT_{\perp}} \cdot \left(\frac{m}{2\pi k T_{\parallel}}\right)^{1/2} \exp\frac{-mv_{\parallel}^2}{2kT_{\parallel}}, \qquad \textbf{(3.6)}$$

where $v_{\parallel}$ and $v_{\perp}$ are the *random* components of the relative velocity parallel and perpendicular to the ion-beam direction, respectively, $T_{\parallel}$ and $T_{\perp}$ are the associated 'temperatures' of the electron beam, and Δ is the detuning velocity. The relative velocity is related to the detuning velocity through the following 'pythagorean' relation:

$$v^2 = v_{\perp}^2 + (\Delta + v_{\parallel})^2. \qquad \textbf{(3.7)}$$

The deviation of the relative energy E_{rel} from the value $E_{rel,0}=m\Delta^2/2$ is

then found to be

$$\delta E_{rel} = m(v^2-\Delta^2)/2 = \delta E_{\perp}+\delta E_{\parallel}\pm 2\sqrt{E_{rel,0}\delta E_{\parallel}}, \qquad \textbf{(3.8)}$$

where $\delta E_{\perp,\parallel}=mv_{\perp,\parallel}^2/2$. For typical electron-beam temperatures of $kT_{\perp}$=100 meV and $kT_{\parallel}$=1 meV, we see from eq.(3.8) that for low energies ($E_{rel}\leq$1 eV), $kT_{\perp}$ determines the energy resolution, whereas for $E_{rel}\geq$10 eV, the last term in eq.(3.8) dominates, and $kT_{\parallel}$ determines the resolution. When low relative energies are considered (i.e. electron-cooling experiments, radiative recombination, dissociative recombination, and low-energy dielectronic recombination), it is therefore of interest to reduce $kT_{\perp}$.

When the guiding solenoid field is kept constant through the cooler, $kT_{\perp}\approx kT_{cath}$, where T_{cath} is the temperature of the cathode. One way to reduce $kT_{\perp}$ is then to reduce the temperature of the cathode. At the MPI Heidelberg, experiments have been made with electron beams produced by laser irradiation of a cold semi-conductor cathode (Habs 1988), but so far, sufficient current for electron-cooler operation has not been achieved. Another way of reducing $kT_{\perp}$ is the so-called adiabatic expansion technique, where the magnetic field strength of the guiding solenoid decreases slowly from the electron gun to the interaction region, leading to an almost proportional decrease in $kT_{\perp}$ (Danared 1993). Since we are now applying the second of these methods, I will describe this in more detail.

Because of the guiding magnetic field, the energy in the transverse motion caused by the finite temperature of the cathode, and possibly imperfections in the fields will be 'stored' in the cyclotron motion of the electrons. The energy in the cyclotron motion is given by the subscript c (for cyclotron)

$$E_c = mr_c^2\omega_c^2/2 = B^2r_c^2e^2/(2m). \quad \textbf{(3.9)}$$

If we assume that the relative change in r_c during one cyclotron oscillation is much smaller than unity (adiabatic motion), the electrons will be able to follow the magnetic field lines, and the magnetic flux through a cyclotron loop will be constant. Hence Br_c^2 is constant. Comparing this to eq.(3.9), we find that E_c changes proportional to the magnetic field. As a measure of the adiabaticity, we introduce the adiabaticity parameter χ, defined by

$$\chi = \frac{1}{B}T\frac{dB}{dt} = \frac{1}{B}\lambda_c\frac{dB}{dz}, \quad \textbf{(3.10)}$$

where T is the cyclotron period, z is the position coordinate along the beam axis, and the distance travelled in the z direction during one period, λ_c, is given by

$$\lambda_c = \left(\frac{8\pi^2 mE_0}{e^2B^2}\right)^{1/2}, \quad \textbf{(3.11)}$$

where E_0 is the electron-beam energy. Numerical simulations using the Hermannsfeldt computer code (Hermannsfeldt 1979) show that the motion remains adiabatic up to $|\chi_{max}|\approx 0.35$. The new ASTRID gun solenoid can give a magnetic field of 2 kG. The magnetic field on axis and the adiabaticity parameter are shown in fig.3.5 for an electron energy of 1 keV and interaction magnetic fields of 100 G and 200 G.

So far, I have assumed that the transverse motion of the electrons consisted solely of the circular motion caused by the random velocity component perpendicular to the solenoid field. This is not strictly true: Even if an electron is launched from the gun with zero

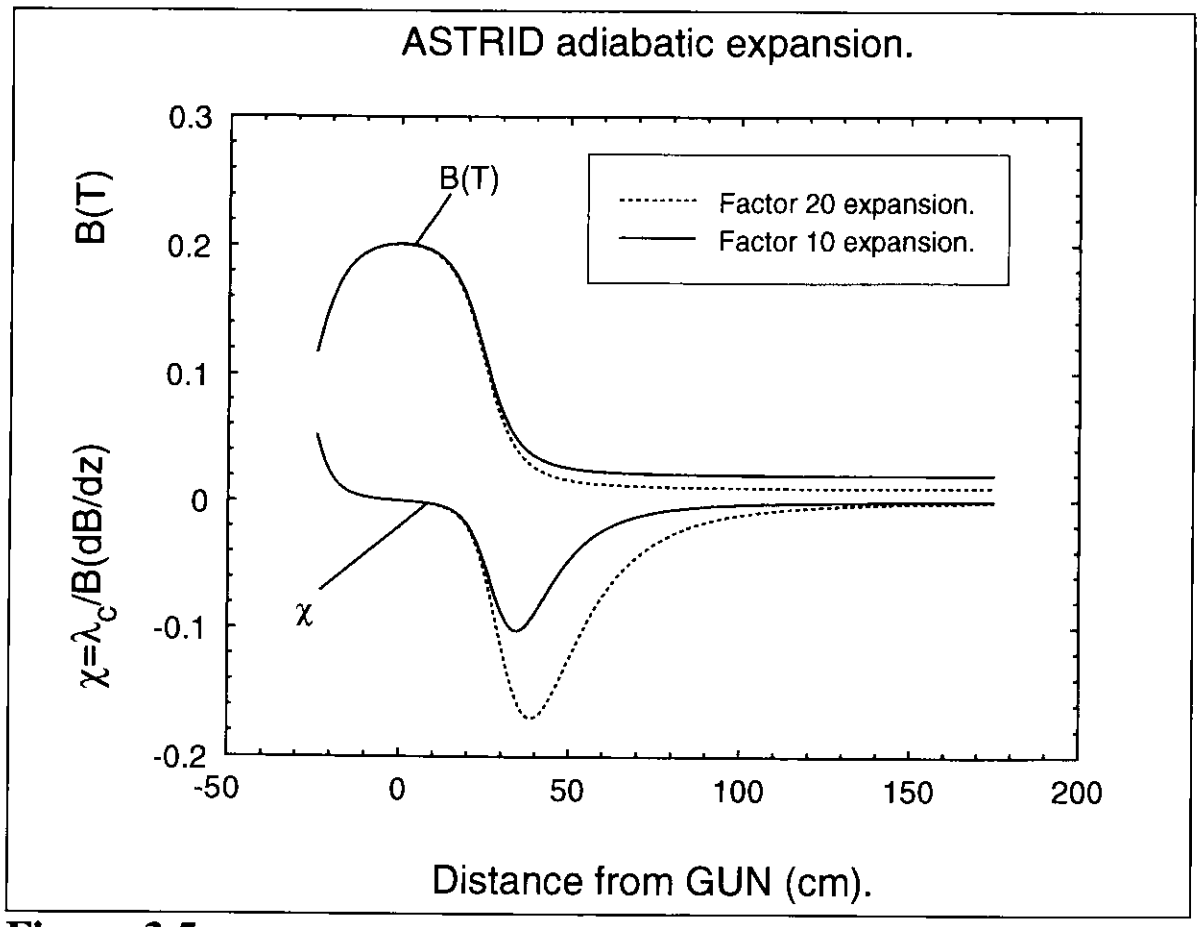

Figure 3.5

transverse velocity, it will start to perform the transverse so-called steady motion. The steady motion is caused by the space-charge electric field, in combination with the solenoid field, and its energy is given by (Poth 1990)

$$E_{ST} = \frac{mr^2\omega_p^4}{8\omega_c^2\gamma^2}, \qquad \textbf{(3.12)}$$

where r is the distance from the center of the beam, ω_p is the plasma frequency, and γ is the relativistic Lorentz factor which is close to one for the energy range of about 1 keV of interest to us. A convenient formula for the steady motion energy yields

$$E_{ST}(eV) = 2.3\cdot10^{-14}\left(\frac{r(mm)n_e(cm^{-3})}{B(G)}\right)^2, \qquad \textbf{(3.13)}$$

where n_e is the electron density. Normally $E_{ST}<<E_c$, but since E_{ST} in the interaction region depends only on the value of the parameters r, B, and n_e in the interaction region, E_{ST} is not affected by the adiabatic expansion and hence sets a limit to the usefulness of this technique. In table 3.1 are shown the cyclotron and steady-motion energies for an electron launched from the gun with a typical transverse energy of 0.13 eV, assuming an interaction-region electron density of $n_e=5\cdot10^6$ cm^{-3}.

Table 3.1

Expansion factor	E_c(meV)	E_{ST}(meV) r=5mm	E_{ST}(meV) r=10mm	E_{ST}(meV) r=15mm	E_{ST}(meV) r=20mm
10	13	0.4	1.7	3.6	*)–
20	6.5	1.7	6.8	15	23

*) *The 1 cm diameter cathode is used. Therefore the radius after a factor of 10 expansion is only 15.8 mm.*

As can be seen from eq.(3.8), also the longitudinal electron-beam temperature plays a role in determining the energy resolution for $E_{rel}\geq1$ eV, in particular if the transverse-energy spread is decreased by adiabatic expansion. We therefore now turn to the longitudinal electron-beam temperature kT_l. Electrons emitted from the hot BaO-coated tungsten cathode obey a spherically symmetric maxwellian velocity distribution with temperature T_{cath}. The ripple on the acceleration voltage causes an increase in the longitudinal-energy spread, as

observed in the laboratory rest frame. What is interesting from the point of view of the experiments is, however, the velocity distribution in the reference frame moving with the average electron velocity. After transforming to this frame of reference, one finds the following longitudinal temperature (Poth 1990):

$$kT_{\parallel} = \frac{(eV_{ripple} + kT_{cath})^2}{4E_0}, \qquad \textbf{(3.14)}$$

where E_0 denotes the electron-beam energy.

The longitudinal temperature given above is, however, not the temperature one finds in the interaction region. In particular, the heating mechanisms, known as longitudinal-longitudinal relaxation and transverse-longitudinal relaxation, play a decisive role in determining the longitudinal beam temperature in the interaction region. These two mechanisms will be described in the following.

When the electrons leave the cathode, their spatial distribution will not be uniform. This means that they will have different potential energies determined by the local density of electrons. The phase-space compression caused by the acceleration as indicated in the above formula will, if the electrons are given sufficient time prior to the acceleration to have these variations in potential energy evolve into kinetic-energy variations, make the effect of this mechanism become negligible. If, however, the acceleration is fast compared to the typical plasma time scale, $\tau_p = 2\pi/\omega_p$, where the plasma frequency is given by $\omega_p = \sqrt{4\pi n_e e^2/m}$, the spatial fluctuations will survive until after the acceleration, whereupon this so-called longitudinal-longitudinal relaxation will lead to an increase of the longitudinal temperature of

approximately $e^2 n_e^{1/3}$ (Kudelainen 1982).

The electron beam now produced has a highly oblate velocity distribution ($kT_{\parallel} << kT_{\perp}$). In this beam elastic scattering among the electrons will gradually transfer the velocity spread from the transverse degrees of freedom into the longitudinal degree of freedom until eventually $kT_{\parallel} = kT_{\perp}$. If the influence of the guiding magnetic field is neglected, the rate of transverse-longitudinal relaxation pr. unit length is given by (Dikansky 1987)

$$\left(\frac{d(kT_{\parallel})}{dz}\right)^{t-1}_{B=0} = \frac{\pi e^3 j L_c C}{E_0}\sqrt{\frac{m}{kT_{\perp}}}, \qquad \textbf{(3.15)}$$

where j is the current density, C is a numerical constant equal to 0.87 for an oblate maxwellian distribution, and L_c is the Coulomb logarithm:

$$L_c = \log\left(\frac{v_{\perp}/\omega_p}{e^2/kT_{\perp}}\right). \qquad \textbf{(3.16)}$$

In more convenient units, the rate of change in the longitudinal temperature is given by

$$\left(\frac{d(kT_{\parallel})}{dz}\right)^{t-1}_{B=0} = \frac{j(A/cm^2)L_c}{E_0(eV)\sqrt{kT_{\perp}(eV)}}\ 8.46\cdot 10^{-3} eV/cm. \qquad \textbf{(3.17)}$$

The magnetic field restricts the transverse motion of the electrons to distances of the order of the cyclotron radius,

$$r_c = \frac{\sqrt{2mkT_\perp}}{eB} = 3.37 \text{ cm } \frac{\sqrt{kT_\perp(eV)}}{B(G)}. \qquad \textbf{(3.18)}$$

For strong magnetic fields, $r_c << n_e^{-1/3}$ and collisions among electrons become improbable, leading to a suppression of the transverse-longitudinal relaxation mechanism. A quantitative measure of this suppression is given by an empirical formula (Kudelainen 1982, Dikansky 1987)

$$\left(\frac{d(kT_\parallel)}{dz}\right)^{t-1} = \left(\frac{d(kT_\parallel)}{dz}\right)^{t-1}_{B=0} \exp\left(-2.8\frac{e^2/r_c}{e^2 n_e^{1/3}+kT_\parallel}\right). \qquad \textbf{(3.19)}$$

I now want to evaluate the effect of these two heating mechanisms for various configurations relevant to the ASTRID electron cooler. We first consider the time scales involved.

We consider as an example an electron beam accelerated to E_0=1000 eV over a distance of d=2 cm and transported s=1 m.

Acceleration time: $\tau_{acc} = 2d/v = 2.2$ ns.

Plasma time scale: $\tau_p = 2\pi/\omega_p = 35 \text{ ns}/\sqrt{n_e/1\cdot10^7 cm^{-3}}$.

Transport time: $\tau_{tr} = s/v = 52$ ns.

Since $\tau_{acc.} << \tau_p$, the acceleration is not adiabatic, and we have to take the longitudinal-longitudinal relaxation into account. As the transport time is of the order of the plasma time scale, we will add the extra longitudinal temperature gradually. A reasonable way to do this is to

set the rate of change of $kT_{\parallel}$ due to longitudinal-longitudinal relaxation equal to

$$\left(\frac{d(kT_{\parallel})}{dz}\right)^{-1} = \frac{e^2 n_e^{1/3}}{v\tau_p} \qquad \textbf{(3.20)}$$

for $z<v\tau_p$ and otherwise zero.

Table 3.2

	Tandem	ASTRID (no ad.exp.)	ASTRID (ad.exp.x 20)	ASTRID (ad.exp.x 10)
Energy(eV)	1000	1000	1000	1000
Ripple peak-peak (V)	0.8	0.8	0.8	0.8
kT_{cath} (eV)	0.11	0.11	0.11	0.11
I (mA)	10	2.8	24.5	12.3
$j^{GUN}(mA/cm^2)$	12.7	1.56	31	15.6
$n_e^{GUN}(cm^{-3})$	$4.1 \cdot 10^7$	$5 \cdot 10^6$	$1 \cdot 10^8$	$5 \cdot 10^7$
$B^{GUN}(G)$	100/200	100/200	2000	2000
$B^{INT.}(G)$	–	–	100	200
$j^{INT.}(mA/cm^2)$	–	–	1.56	1.56
$n_e^{INT.}(cm^{-3})$	–	–	$5 \cdot 10^6$	$5 \cdot 10^6$
$kT_{\parallel}^{GUN}(eV)$	$6.5 \cdot 10^{-5}$	$6.5 \cdot 10^{-5}$	$6.5 \cdot 10^{-5}$	$6.5 \cdot 10^{-5}$
$kT_{\parallel}^{INT.}(eV)$ *)	$4.5/4.1 \cdot 10^{-4}$	$1.3/1.2 \cdot 10^{-4}$	$2.5 \cdot 10^{-4}$	$1.6 \cdot 10^{-4}$
$kT_{\perp}(eV)$	0.11	0.11	0.0055	0.011

*) *Halfway through the electron cooler.*

If we now add the contributions from longitudinal-longitudinal and transverse-longitudinal relaxation, we find the total rate of change of the longitudinal temperature. A numerical integration can then be performed to find the longitudinal temperature as a function of the distance from the electron-gun anode. The results of this calculation for some relevant configurations are given in table 3.2. Note that due to the lower electron density in the ASTRID experiments as compared to the Tandem experiments, the longitudinal temperature is expected to be lower.

Figure 3.6 shows the calculated electron beam temperatures for the ASTRID electron cooler in the case of a factor 10 adiabatic expansion as a function of the longitudinal-position coordinate z.

The electron-beam temperatures, $kT_{\parallel}$ and $kT_{\perp}$, can be deter-

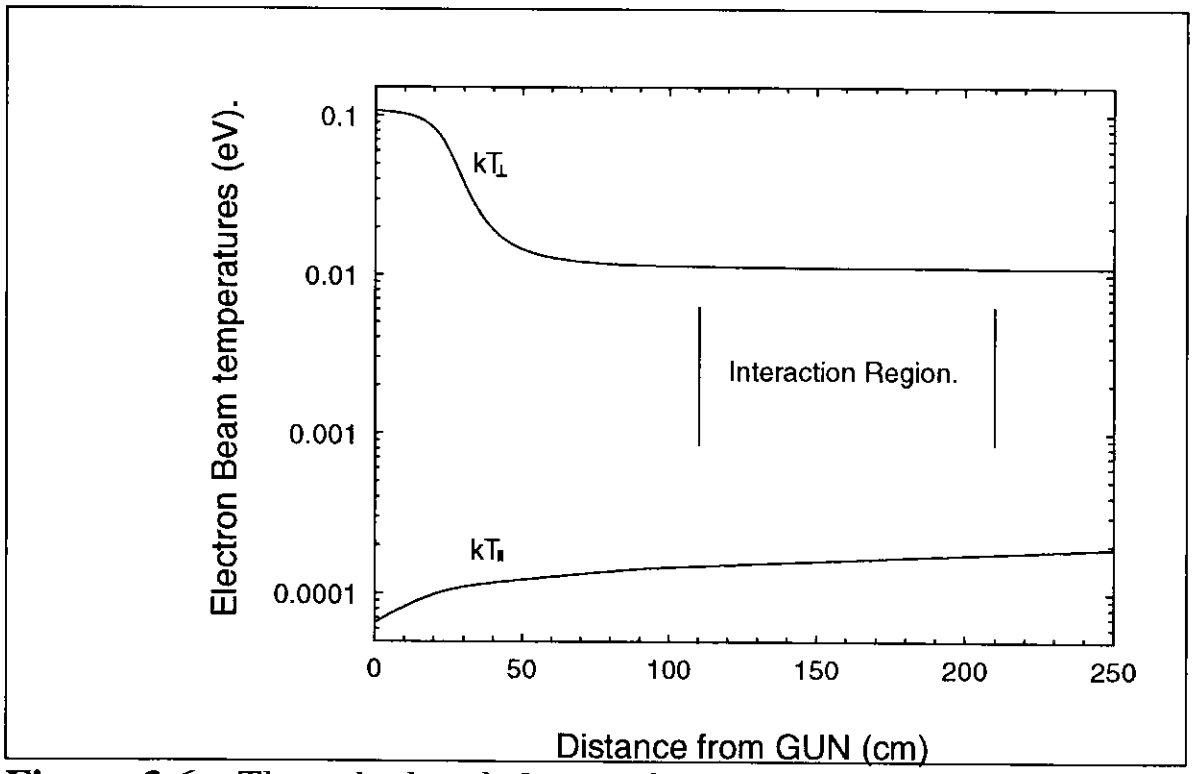

Figure 3.6 *The calculated electron beam temperatures for ASTRID with factor 10 adiabatic expansion.*

mined from the experimental spectra of dielectronic recombination. When a narrow isolated DR resonance is considered, it can be assumed that $\sigma(v)$ is just a δ function. In this case, the integral in eq.(3.5), with f given by eq.(3.6) can be solved analytically in the neighborhood of the resonance, giving $\langle v\sigma \rangle$ as a function of the detuning Δ or, equivalently, as a function of $E_{rel,0}=m\Delta^2/2$

$$\langle v\sigma \rangle(E_{rel,0}) = \text{constant}\cdot\exp\left(-\frac{E_{rel,0}}{kT_{\parallel}}-\frac{E_{res}}{kT_{\perp}}+\frac{E_{rel,0}}{kT_{\parallel}(1-kT_{\parallel}/kT_{\perp})}\right)$$
$$\cdot\left[\operatorname{erf}\left(\left|\sqrt{\frac{E_{res}}{kT_{\parallel}}(1-kT_{\parallel}/kT_{\perp})}-\sqrt{\frac{E_{rel,0}}{kT_{\parallel}(1-kT_{\parallel}/kT_{\perp})}}\right|\right)\right. \qquad \textbf{(3.21)}$$
$$\left.-\operatorname{erf}\left(\sqrt{\frac{E_{res}}{kT_{\parallel}}(1-kT_{\parallel}/kT_{\perp})}+\sqrt{\frac{E_{rel,0}}{kT_{\parallel}(1-kT_{\parallel}/kT_{\perp})}}\right)\right],$$

where E_{res} is the resonance energy, and erf is the error function defined as

$$\operatorname{erf}(x) = \frac{2}{\sqrt{\pi}}\int_0^x e^{-u^2}du. \qquad \textbf{(3.22)}$$

The parameters E_{res}, constant, $kT_{\perp}$, and $kT_{\parallel}$ can then be varied to obtain the best fit to the data points. Figure 3.7 shows such a fit for the electron beam used in the tandem accelerator experiments. The resonance was $O^{6+}(1s2s\ ^1S) + e^- \rightarrow O^{5+}(1s2p(^1P)11l)$, and the result of the fit was $kT_{\parallel}=10(5)\cdot10^{-4}$eV and $kT_{\perp}=0.135(10)$eV. In fig.3.8 is shown the corresponding electron-beam-temperature determination for the Heidelberg electron beam performed with a C^{4+} beam. We used the

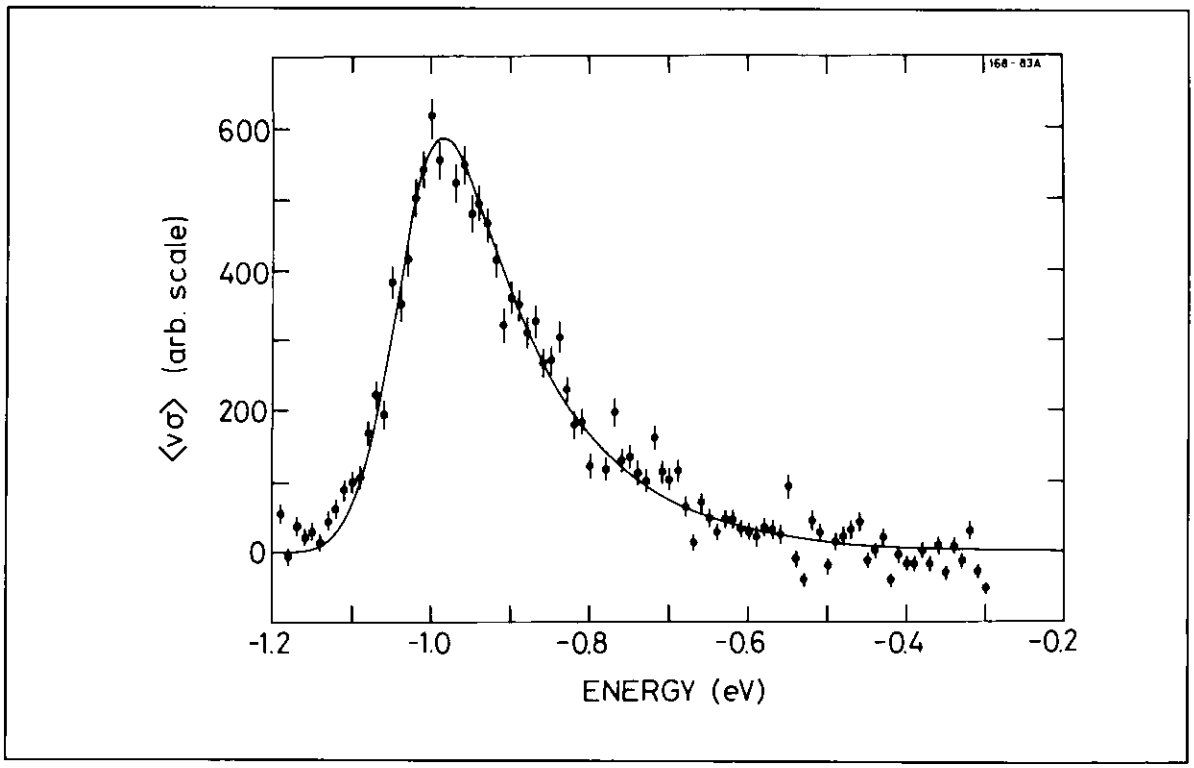

Figure 3.7 *Data points and fit function at the resonance used for the tandem temperature fit. (The negative energy sign just means that the electrons moved slower than the ions).*

resonance $C^{4+}(1s2s\ ^3S) + e^- \rightarrow C^{3+}(1s2s(^1P)7l)$ and found the temperatures $kT_\parallel = 6.3(5)\cdot10^{-4}$eV and $kT_\perp = 0.134(10)$ eV. Due to the larger l splitting for this resonance, a fit was made to *two* δ-shaped resonances. Furthermore, a first-order polynomial was introduced to take into account a slope in the 'background recombination' signal probably caused by the next resonance in the spectrum.

When comparing the measured temperatures for the tandem experiments with the calculated ones, we find reasonable agreement. The slightly higher value for $kT_\perp$ can be ascribed to non-uniformity of the solenoid field, but also the ion-beam divergence plays a role since different ions will have slightly different angles with respect to the electron beam, thereby contributing to the spread of relative transverse velocities. Concerning $kT_\parallel$, the effect of the finite size of the ion beam

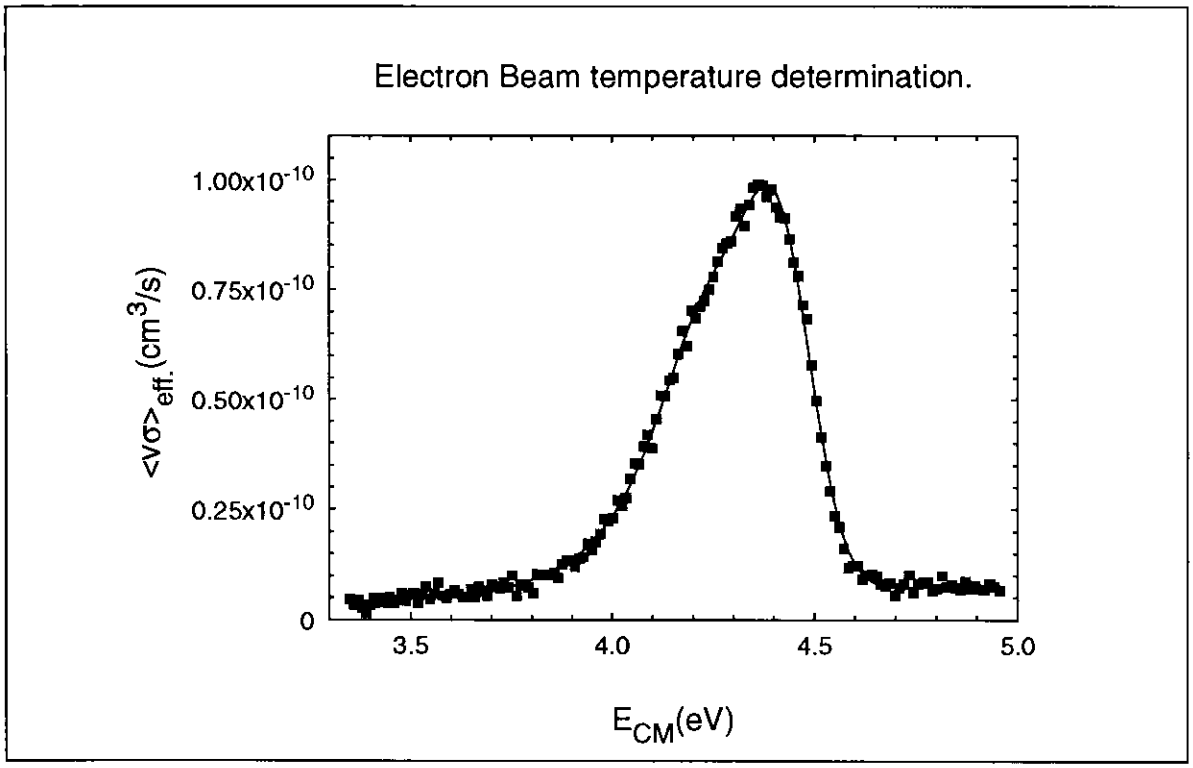

Figure 3.8 *Electron-beam-temperature determination for the TSR electron beam using a C^{4+} beam.*

comes into play since different transverse positions correspond to different values of the electron-beam space-charge potential given by

$$V_{sp} = \frac{I(A)}{\sqrt{E_0(eV)}} \cdot 1.5 \cdot 10^4 \left[\left(\frac{r}{a} \right)^2 - 1 + 2\ln\left(\frac{a}{R} \right) \right], \qquad (3.23)$$

where a is the electron-beam diameter and R is the diameter of the vacuum chamber. A 1 mm ion-beam radius combined with a 1 mm displacement can then give about 1 V variation in electron space charge across the ion beam for a 10 mA, 1 keV electron beam. This is equivalent to an increase in the peak-to-peak ripple on the acceleration voltage of 1 V. Inserting this in the calculations presented above leads to an increase of almost 50% in $kT_{\parallel}$. Finally, it is important to bear in mind that electron-beam temperatures measured

with this technique will always be upper limits since any effects of 'non-δ likeness' (e.g finite energy width or *l* splitting) will lead to apparently higher beam temperatures.

3.3. Electron cooling

Let us consider the electron beam as seen from a reference frame moving with the average electron velocity. If an ion enters this free electron plasma from any direction, it will experience a friction force directed opposite to its velocity vector. The force is known as the drag force and is caused by large-impact-parameter Rutherford scattering between the ions and the electrons. In the single-pass experiments, the influence of the drag force on the recombination experiments could be neglected, but in the storage ring, where the ions pass through the electron cooler several hundred thousand times per second, the accumulated effects of all these passages may be quite significant. In this section, the effects of the drag force relevant to the ion-electron recombination experiments will be discussed qualitatively, and results of cooling of a 4 MeV D^+ beam in ASTRID will be presented.

When the ions and electrons are tuned to the same average velocity, the slower ions are accelerated, and the faster ones are decelerated, leading to a narrowing of the longitudinal velocity distribution of the ions. This is known as longitudinal electron cooling. The process is especially interesting when the initial temperature of the ion beam is so high that the assumption we made in the previous section, that the relative velocity distribution can be well approximated

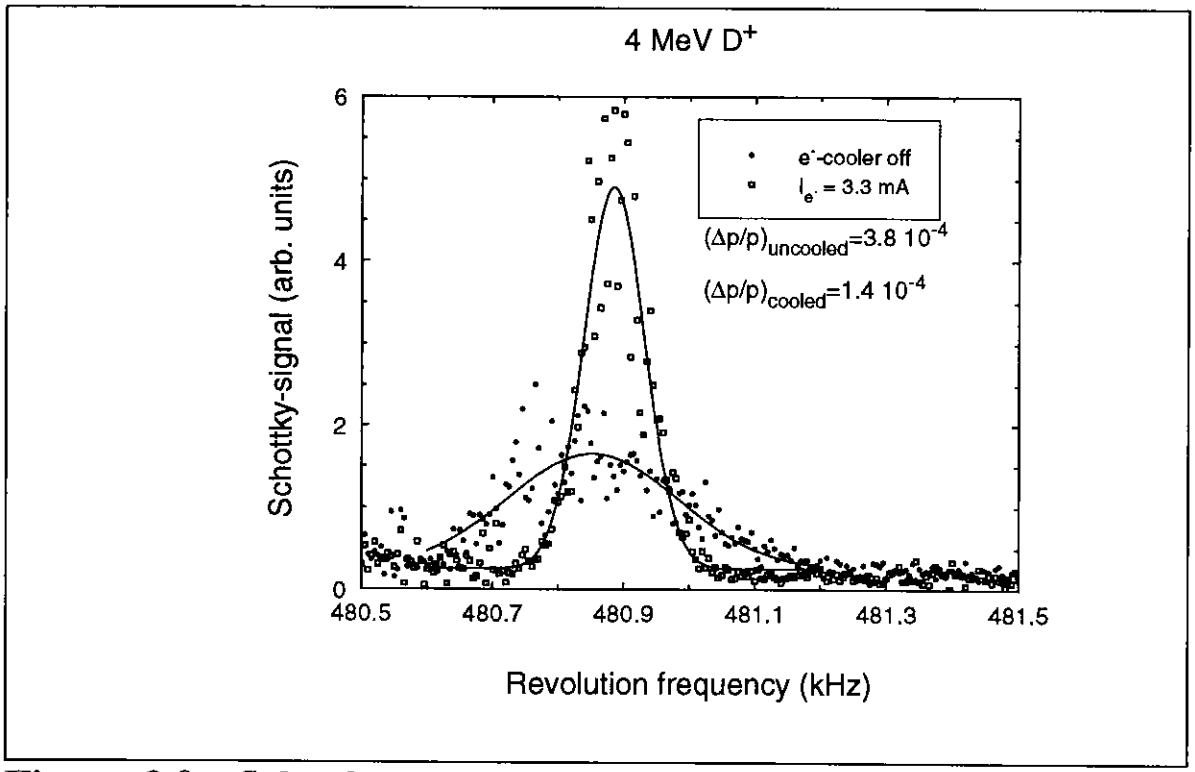

Figure 3.9 *Schottky-noise spectra with gaussian fits of a 4 MeV D^+ beam stored in ASTRID. The squares show the cooled beam, and the dots show the uncooled ion beam.*

by the electron velocity distribution, no longer holds. In this situation, electron cooling of the ions can practically eliminate the influence from the ion-beam velocity distribution. In fig. 3.9 is shown the Schottky-noise spectrum of a 4 MeV D^+ beam with (squares) and without (dots) electron cooling. This spectrum is the power spectrum of the electrostatic pick-up signal from a cylindrical electrode through which the ion beam passes. Any density fluctuations in the ion beam give rise to a signal at the revolution frequency and its harmonics. The Schottky-noise spectrum hence gives the distribution of revolution frequencies of the ions. To deduce the relative momentum spread from the relative frequency spread, one must divide by the off-momentum factor given by (Poth 1990),

$$\eta = 1-(v/c)^2-\alpha, \tag{3.24}$$

where the momentum compaction factor α is defined as

$$\alpha = \frac{\Delta C/C}{\Delta p/p}, \tag{3.25}$$

where C is the circumference of the orbit of a particle with momentum p. For standard ASTRID operation, $\alpha = 0.053$ (Møller 1994), leading to $\eta = 0.943$ for a 4 MeV D^+ beam. For the cooled beam from fig.3.9, we found $\Delta p/p=1.44\cdot10^{-4}$, where Δp is defined as the standard deviation from the mean value of p. Introducing a 'temperature' in analogy to the electron-beam case, we find $kT_{\parallel ion}=82$ meV, which is much higher than the expected longitudinal *electron* beam temperature of about 1 meV. We see that we do not get complete temperature equilibration between the ions and the electrons. The heating mechanism responsible for this difference is the intra-beam scattering of the ion beam. In the case of equilibrium between intra-beam scattering and electron cooling, $\Delta p/p$ is proportional to $N_i^{0.4}$, where N_i is the number of stored ions (Poth 1990). In table 3.3 is shown $\Delta p/p$ for three different ion intensities, and we see that the $N_i^{0.4}$ dependence is confirmed.

When there is a detuning of the two beam velocities, the drag force will have the same direction for all ions, leading to acceleration or deceleration of the entire ion beam. This can be an obstacle for measuring recombination rate coefficients at very low relative energies, where the drag force is at maximum. This problem is normally circumvented by modulating the electron energy between cooling energy (zero detuning) and the energy at which one wants to measure.

Table 3.3

Ion current $I_i(\mu A)^*$	$\Delta p/p$	$\Delta p/p \cdot (I_i(\mu A))^{-0.4}$
5	$1.7 \cdot 10^{-4}$	$8.9 \cdot 10^{-5}$
1	$6.9 \cdot 10^{-5}$	$6.9 \cdot 10^{-5}$
0.5	$5.5 \cdot 10^{-5}$	$7.3 \cdot 10^{-5}$

**) The absolute value of the ion current is only known within a factor of two, but by monitoring the production of neutrals, a relative current measurement with an uncertainty of about 2% could be performed.*

We measured the drag force as a function of the detuning by setting a certain detuning and then watching the drift of the peak in the Schottky spectrum as a function of time. The result of this is shown in

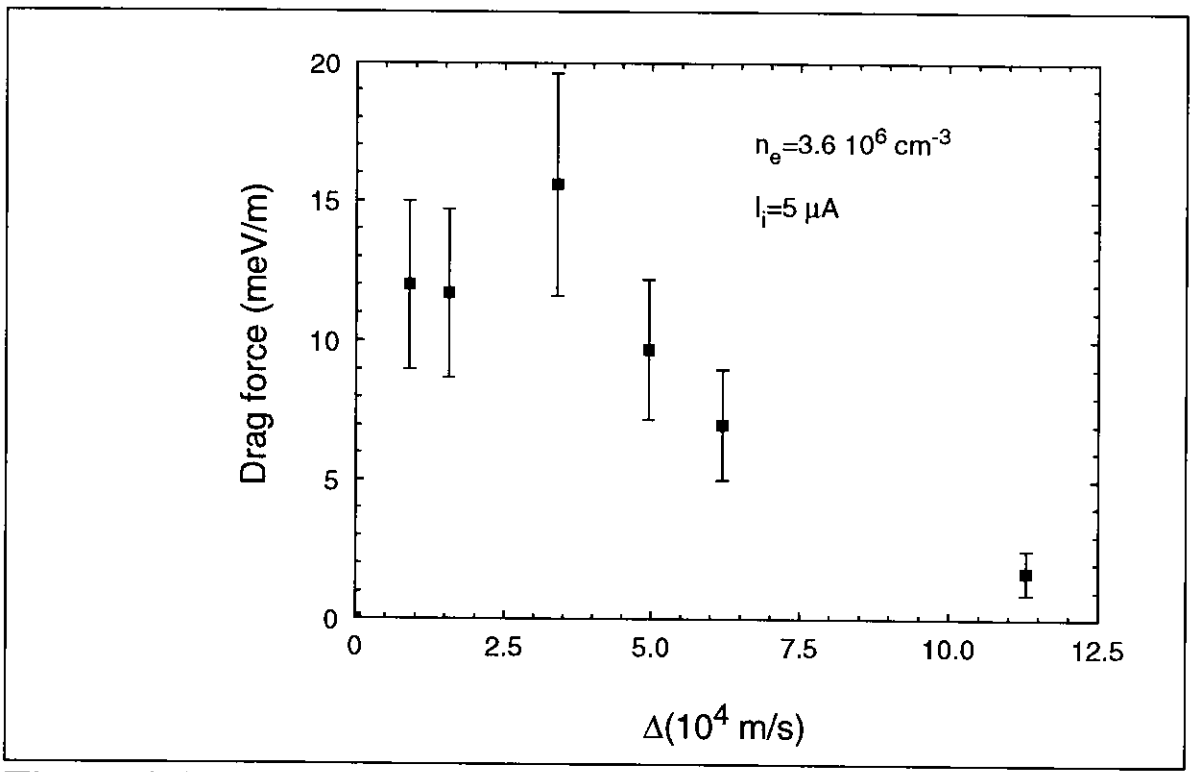

Figure 3.10 *The measured drag force as a function of the detuning velocity Δ.*

fig.3.10.

So far, we have considered only effects of the drag force in the longitudinal direction, but a damping of the transverse motion also takes place. This damping leads to lower transverse ion-beam temperature, smaller beam size, and elimination of the loss of stored particles due to multiple scattering in the residual gas. This last point is illustrated in fig.3.11, where we see that the storage lifetime of a D^+ beam is increased by more than one order of magnitude by applying electron cooling.

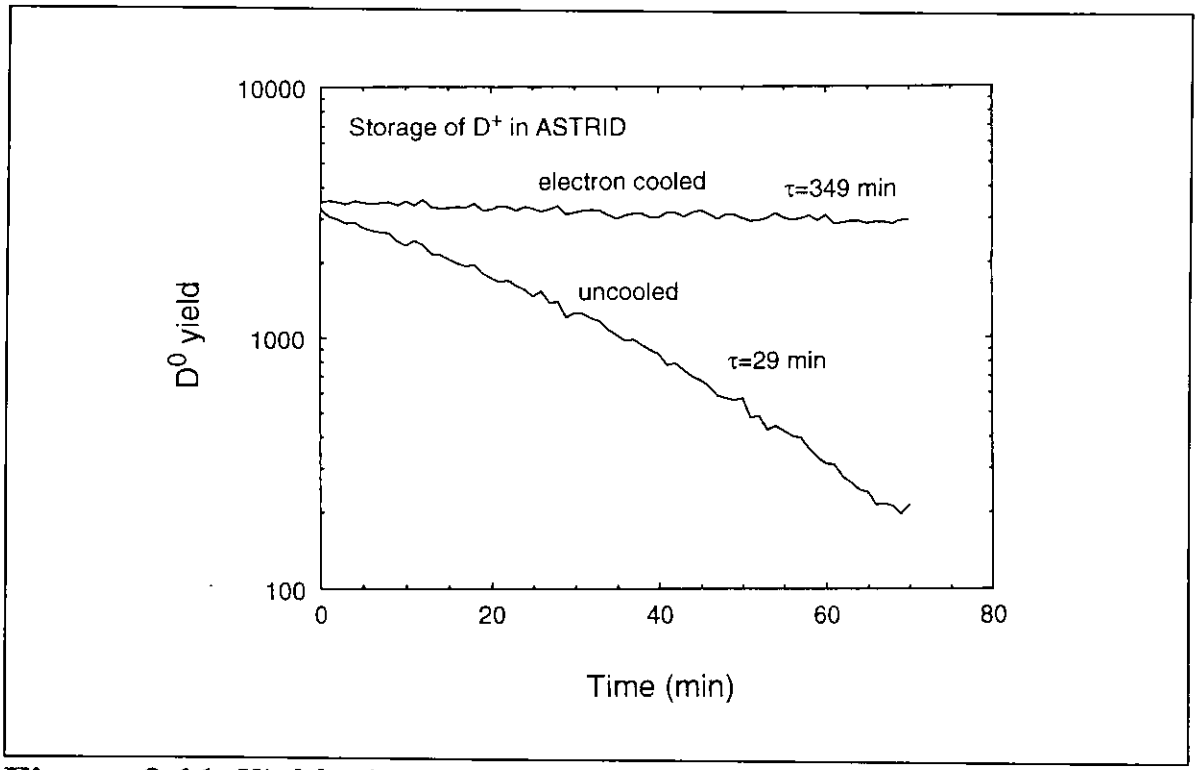

Figure 3.11 *Yield of neutrals from stored D^+ beam as a function of time after injection. The upper curve was obtained by applying electron cooling ($n_e=3.6\cdot10^6$ cm^{-3}).*

H Danared (1993) Nucl.Instr&Methods ***A335*** *397*

N S Dikansky et al.(1987) Proc. XIII Intern. Conf. on High Energy Accel.- Nauka ***1*** *330.*

D C Griffin (1989) Physica Scripta ***T28*** *17*

D Habs, J Kramp, P Krause, K Matl, R Neumann, and D Schwalm (1988) Physica Scripta ***T22****, 269*

W Hermannsfeldt, SLAC report 226 (Stanford 1979).

V I Kudelainen, V A Lebedev, I N Meshkov, V Parkhomochuk, and B N Sukhina (1982) Sov.Phys.JETP ***56*** *1191.*

S P Møller (1994) Private communication.

H Poth (1990) Physics Reports ***196*** *135.*

4. Radiative Recombination

In this chapter, the process of radiative recombination (RR) is being discussed, and results of the tandem accelerator single-pass experiments are presented. Section 4.1 on RR for fully stripped ions serves as an introduction to the two following sections on RR for non-fully stripped ions (sec.4.2) and on laser-induced recombination (sec.4.3).

The formal prescription of RR is

$$X^{q+} + e^{-} \rightarrow X^{(q-1)+}(nl) + h\nu, \qquad \textbf{(4.1)}$$

where q is the ion charge in units of the elementary charge e, n and l are the principal and orbital angular momentum quantum numbers of the captured electron, respectively, and hν is the energy of the photon emitted.

4.1 RR for fully stripped ions

We start by considering the case of the initial-state ion being a bare nucleus. For this case, an approximative calculation of the RR cross section was performed by Kramers (Kramers 1923). The Kramers formula gives the cross section for capture to a final state with principal quantum number n,

$$\sigma_n = 2.10 \cdot 10^{-22} \mathrm{cm}^2 \cdot \frac{Z^4 (e^2/(2a_0))^2}{n E_{rel} (Z^2 (e^2/(2a_0)) + n^2 E_{rel})}, \qquad \textbf{(4.2)}$$

where Z is the nuclear charge in units of e, and a_0 is the Bohr radius.

The derivation of this formula is based on the old quantum mechanics of Bohr and Sommerfeld. The idea is to consider the classical wavelength distribution of the light emitted from an initially free electron, accelerated in the Coulomb field of the nucleus. This wavelength distribution is then modified to take into account the discrete energy levels of the final state, as well as the quantization of light introduced through Einstein's formula,

$$E_{photon} = h\nu = hc/\lambda. \qquad \textbf{(4.3)}$$

With these restrictions, the continuous classical distribution is modified to a series of discrete values. In accordance with the correspondence principle, it is assumed that the integral of the energy emitted in the form of light would be the same as found in the classical calculation. With this assumption, the light emitted in a certain wavelength interval in the classical calculation, can now be associated with radiative recombination into a bound state with a certain principal quantum number *n*. This procedure leads to the Kramers formula.

After the development of the modern quantum mechanics, exact calculations of the RR cross section for fully stripped ions were performed (Stobbe 1930). These give rise to corrections to the Kramers formula described via the so-called 'Gaunt factors' g_{nl} (Gaunt 1930), defined as the exact cross section divided by the cross section given by the Kramers formula. The *l*-averaged Gaunt factors may be expressed

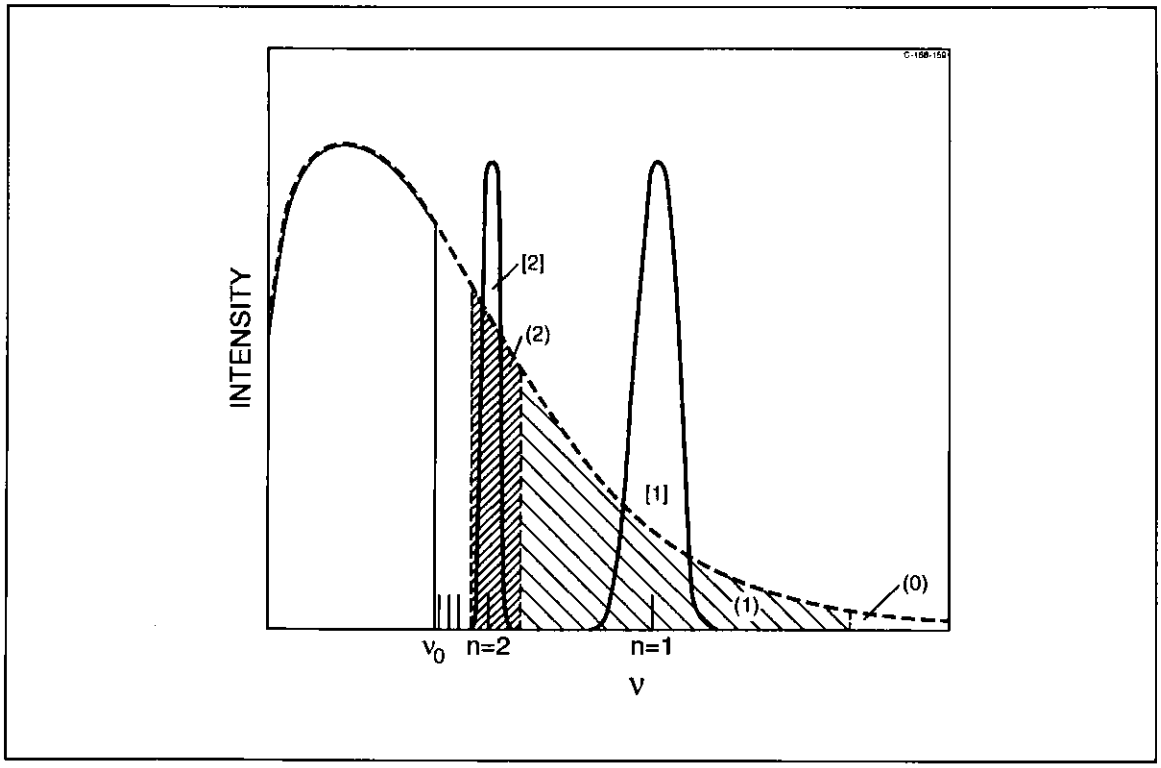

Figure 4.1 *Illustration of Kramers's discretization principle of the emitted radiation.*

by the following asymptotic expansion (Seaton 1959, Griffin 1989):

$$\bar{g}_n = 1 + 0.1728n^{-2/3}(u+1)^{-2/3}(u-1) - 0.0496n^{-4/3}(u+1)^{-4/3}(u^2+(4/3)u+1) + \ldots , \quad (4.4)$$

where $u=E_{rel}/(h\nu-E_{rel})$.

From the quantum mechanical point of view, RR is a radiative transition from a continuum state to a bound state described by the following transition matrix element:

$$T_{fi} = \langle \varphi_{nl}, \bar{k}\rho | H_{int} | \psi_{\bar{\kappa}}^{+}, \text{vac} \rangle, \quad (4.5)$$

where the final state is a bound state, φ_{nl}, of the H-like ion plus a photon with wave vector $\bar{k}$ and polarization $\bar{e}_{\bar{k}\rho}$. The initial state is a 'free' electron (distorted by the infinite-ranging Coulomb potential) and

the vacuum state of the electromagnetic field. The interaction Hamiltonian takes on the form (Weissbluth 1978)

$$H_{\text{int}} = -\frac{e}{mc}\cdot\bar{e}_{\bar{k}\rho}\cdot\bar{p}\left(a_{\bar{k}\rho}e^{i\bar{k}\bar{r}} + a^{+}_{\bar{k}\rho}e^{-i\bar{k}\bar{r}}\right), \qquad (4.6)$$

where $a_{\bar{k}\rho}$ and $a^{+}_{\bar{k}\rho}$ are the photon annihilation and creation operators, respectively. For radiative recombination, only the creation operator yields non-zero matrix elements. For photoionization, which is the inverse process, only the annihilation operator contributes.

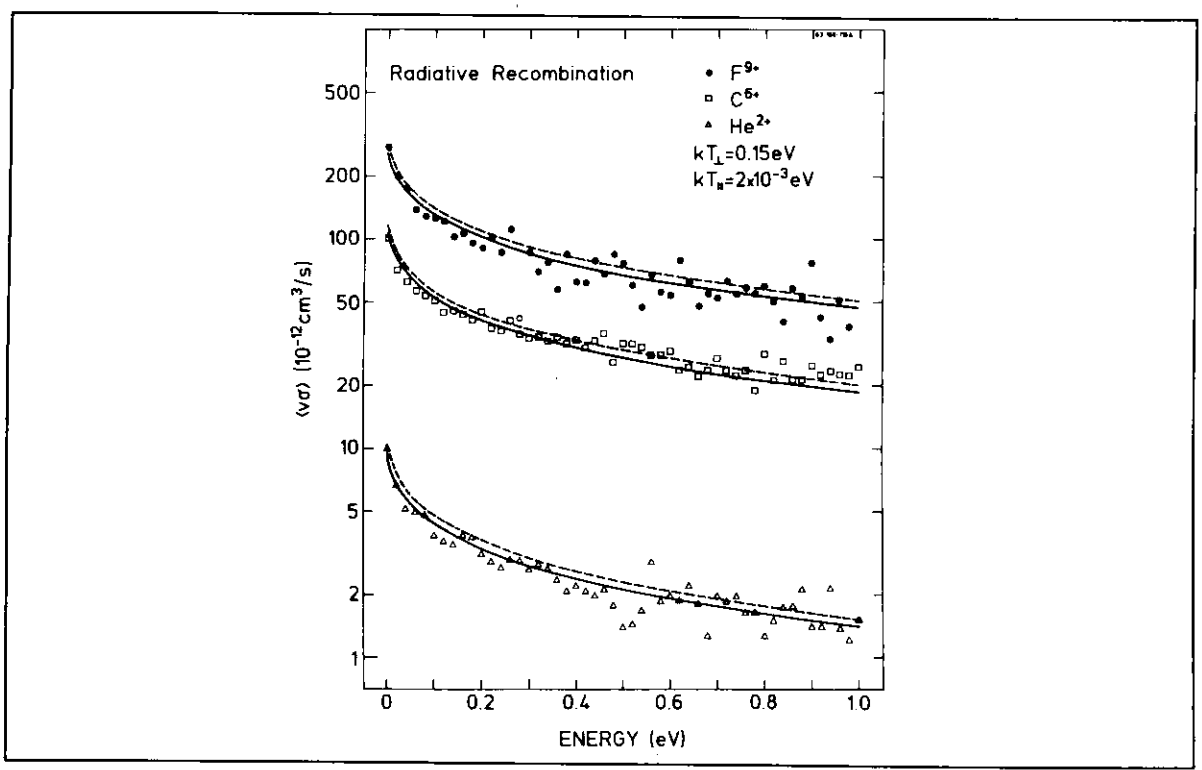

Figure 4.2 *RR rate coefficient as a function of relative energy for He^{2+}, C^{6+}, and F^{9+}. Kramers's result with (full curve) and without (dashed curve) Gaunt corrections (Andersen 1990a).*

A detailed derivation of the cross section as a function of the relative energy from evaluation of the matrix elements of eq.(4.5) is presented in the thesis of Jakob Bolko (Bolko 1991).

Measurements of RR for He^{2+}, C^{6+}, and F^{9+} in the Aarhus single-pass tandem experiment (Andersen 1990a) confirm these calculations (see fig.4.2) when the effect of field ionization caused by the electric charge-state analyzer field is taken into account. Other experimental studies, performed at the Test Storage Ring (TSR) at the Max Planck Institute Heidelberg, indicate discrepancies of up to 50% for C^{6+} and Cl^{17+} (Wolf 1991), the measured rate coefficient being larger than the theoretically predicted value.

4.2 RR for non-fully stripped ions

For non-fully stripped ions, calculations become more complicated since the final state is no longer a hydrogenic one. However, for states with relatively high n quantum number, the dominating contribution to RR comes from states with $l \geq 2$, and the hydrogenic approximation may be applicable. Since the decrease in the cross section with increasing n given by the Kramers formula is slow for relative energies close to zero, the total cross section will be dominated by contributions from states for which the hydrogenic approximation is good. It is therefore reasonable to use the hydrogenic approximation for the total radiative recombination cross section $\sum_{n}^{n_{\text{limit}}} \sigma_n$, where the summation is restricted to non-occupied levels. It is, however, not clear which charge should be entered in the Kramers formula for this situation. Electrons with high angular momentum will not penetrate the core, and one will expect the effective charge that one should use to be equal to the ion charge. For low-l electrons, however, the incoming electron may penetrate the ion core, leading to an effective charge

higher than the ion charge q and smaller than the nuclear charge Z. A theoretical discussion of the *nl* dependence of the effective charge derived from Hartree-Fock calculations is given by McLaughlin and Hahn (MacLaughlin 1991), Sunggi and Lin (Sunggi 1991), and Kim and Pratt (Kim 1983). In our measurements, no information on the final state of the recombination products was available. We could, however, deduce an average effective charge q_{eff} by comparing our data to the result of hydrogenic calculations with different values of the charge inserted in the Kramers formula. With this procedure, good agreement with experiments has been found for the H-like ions C^{5+}, O^{7+}, and F^{8+}, as well as for Li-like O^{5+} and Si^{11+}, in all cases using $q_{eff}=q$ (Andersen 1990b),[II]).

Figure 4.3 shows the result of our measurement of the RR rate coefficient for the O-like Si^{6+} ion [II]. Also shown in this figure are the results of the hydrogenic approximation using $q_{eff}=q=6$ and $q_{eff}=9$, respectively. We see that in order to reproduce our experimental data, $q_{eff}=9$ should be used. The fact that $q_{eff}>q$ we take as evidence of incomplete screening. For F^{3+} [V], we also observed incomplete screening.

Since it has been found that for H-like and Li-like ions, one should use $q_{eff}=q$, whereas for C-like and O-like ions $q_{eff}>q$, it is tempting to ascribe the effect of incomplete screening to the presence of 2p electrons in the initial-state ion. This observation is probably related to the fact that p-wave functions extend to larger distances from the nucleus than s-wave functions.

Another measurement of RR for non-fully stripped ions was performed by Müller et al. on U^{28+} ions (Müller 1991). They found a maximum rate coefficient of $r \approx 1 \cdot 10^{-7} cm^3\ s^{-1}$. This was compared to a